Journal of
Synchrotron
Radiation

ISSN 0909-0495

Received 17 July 2007
Accepted 26 November 2007

Fabrication of high-aspect-ratio Fresnel zone plates by e-beam lithography and electroplating

Y. T. Chen,[a,b] T. N. Lo,[a] C. W. Chiu,[a] J. Y. Wang,[a] C. L. Wang,[a] C. J. Liu,[a] S. R. Wu,[a,c] S. T. Jeng,[a,d] C. C. Yang,[a,d] J. Shiue,[a] C. H. Chen,[a] Y. Hwu,[a,c,d,e]* G. C. Yin,[e] H. M. Lin,[b] J. H. Je[f] and G. Margaritondo[g]

[a]Institute of Physics, Academia Sinica, Taipei 115, Taiwan, [b]Department of Materials Engineering, Tatung University, Taipei 104, Taiwan, [c]Department of Engineering Science and System, National Tsing Hua University, Hsinchu 300, Taiwan, [d]Institute of Optoelectronic Sciences, National Taiwan Ocean University, Keelung 202, Taiwan, [e]National Synchrotron Radiation Research Center, Hsinchu, Taiwan, [f]X-ray Imaging Center, Pohang University of Science and Technology, Pohang, Korea, and [g]Ecole Polytechnique Fédérale de Lausanne (EPFL), CH-1015 Lausanne, Switzerland.
E-mail: phhwu@sinica.edu.tw

The fabrication of gold Fresnel zone plates, by a combination of e-beam lithography and electrodeposition, with a 30 nm outermost zone width and a 450 nm-thick structure is described. The e-beam lithography process was implemented with a careful evaluation of applied dosage, tests of different bake-out temperatures and durations for the photoresist, and the use of a developer without methylisobutylketone. Electrodeposition with a pulsed current mode and with a specially designed apparatus produced the desired high-aspect-ratio nanostructures. The fabricated zone plates were examined by electron microscopy and their performances were assessed using a transmission X-ray microscope. The results specifically demonstrated an image resolution of 40 nm.

© 2008 International Union of Crystallography
Printed in Singapore – all rights reserved

Keywords: Fresnel zone plate; e-beam lithography; electrodeposition; nanofabrication; X-ray microscope.

1. Introduction

The Fresnel zone plate (FZP) is a most effective device for concentrating X-ray beams (Attwood, 1999). Its focusing efficiency depends on the quality of its structure consisting of alternating concentric rings that modulate the beam wavefront to produce constructive interference at the focal point. Because of its high efficiency, the FZP is the key optical component in full-field transmission X-ray microscopy (TXM) (Yin *et al.*, 2006) as a magnifying device of the X-ray image. In scanning X-ray microscopy the FZP effectively transforms the incoming X-ray beam into a microprobe or nanoprobe (Hambach *et al.*, 2001).

Since the resolution of FZPs is proportional to the smallest zone width, accurate fabrication is required to improve the resolution of either type of microscopy. On the other hand, the high penetration of hard-X-ray photons requires FZPs with thick structures of high-*Z* metals, creating additional fabrication challenges. For example, Au FZPs must be at least 450–500 nm thick to be effectively used for multi-keV X-rays.

In the present work we have implemented an optimized nanofabrication approach to produce Au FZPs with a (smallest) outermost zone width of 30 nm and a thickness >450 nm. The process involves several state-of-the-art nanofabrication procedures. Each step is fine-tuned to produce high-density nanostructures with high aspect ratios of >10 (Lo *et al.*, 2007).

The first component in the fabrication process was electron-beam (e-beam) lithography (EBL), which is capable of defining patterns with the required high resolution (<10 nm) and of dealing with the under-cut problem, which is particularly serious for high-aspect-ratio structures. The desired results were obtained with careful optimization of the dose parameters and characterization of the initial pattern design. Furthermore, we operated the e-beam writer at a high accelerating voltage, ∼100 keV, not common in EBL, strongly reducing the backscattering-related inaccuracy (Anderson *et al.*, 2001; Lo *et al.*, 2007). The combination of high resolution and large overall dimensions, often >100 μm, is an additional challenge while using e-beam writing as a FZP fabrication step; in our case, high resolution was achieved over a wide area without stitching and the related errors.

The development of the EBL-defined resist pattern for high-aspect-ratio nanostructures requires a different approach than with standard lithography. A typical developer for high-resolution patterning is a mixture of MIBK (methylisobutylketone) and IPA (2-propanol). However, when the feature size is below 50 nm, this solution seriously attacks the unexposed part of the photoresist (Olzierski & Raptis, 2004; Manjkow *et al.*, 1987). Extensive tests proved that mixing IPA

and water does produce sufficient contrast and the required pattern precision (Brambley & Bennett, 1996; Yasin *et al.*, 2002).

The second component of our fabrication procedure was electrodeposition. The production of Au structures with high density and high aspect ratio required a special electrodeposition approach. The dimension of the smallest zone was shorter than the diffusion length of Au ions in the solution (typically of the order of μm); the need to produce different high-density zone widths was another complicating factor. An accurate control was required of the critical electrodeposition parameters, such as the current density, the deposition time and the deposition mode.

The overall bath design and specifically the optimization of parameters such as the anode shape and the distance and surface area ratio between anode and cathode was also quite critical (Jangidze *et al.*, 2007). We empirically found suitable solutions based on our experience in the fabrication of high-aspect-ratio structure by localized electrochemical deposition (LECD) (Said, 2003; Seol *et al.*, 2005). We discovered that an anode and a cathode with similar shapes and areas significantly improved the final products.

The devices so fabricated were extensively characterized: tests in the full-field imaging mode demonstrated that the target FZP parameters and performance were achieved, including a 30 nm outermost zone width and an aspect ratio of >15. Further improvements of the process are underway and we expect significant improvements of the critical parameters in the near future.

2. Experimental procedure

The FZP structures were fabricated on research-grade Si(100) wafers. To reduce unwanted X-ray absorption by the Si substrate, FZP structures are normally produced on thin membranes. The membrane must possess the required mechanical strength to guarantee device reliability. We met this requirement with a process producing a thin SiN membrane. The first step was to use low-pressure chemical vapor deposition to deposit a layer of SiN_x, typically 1 μm thick, on both sides of the Si wafer and to produce low-stress (100 MPa) SiN_x of sufficient strength. Before the conductive ~100 nm Au layer, a buffer layer of Cr, ~10 nm, was deposited on one side by electron beam epitaxy to improve the adhesion.

A 3 mm × 3 mm window was then created on the 'back' side of the Si substrate (the side of the final FZP patterns), to expose the front-side SiN_x/Cr/Au layer. The window was obtained by first using a 365 nm I-Line UV aligner on a S1813 photoresist and then reactive ion etching to remove the back-side SiN_x. The Si substrate within the window was then chemically removed by exposure to a 27% KOH solution for 5 h, leaving a thin SiN_x/Cr/Au membrane.

We used two types of e-beam resists in the 950 PMMA (polymethylmethacrylate with molecular weight of 950, MicroChem Co.) series, A6 and A9. They were spin coated on the Au layer and baked at either 408 K for 2 h or at 453 K for 24 h to produce a resist layer of thickness ~450 nm (A6) and ~1000 nm (A9). The FZP pattern was defined on the resist by an e-beam writer (Elionix ELS-7000) operating at the aforementioned high applied voltage of 100 keV and at a current of 10 pA. The patterns were developed with a 7:3 mixture of IPA and water for 60 s to completely remove the exposed photoresist.

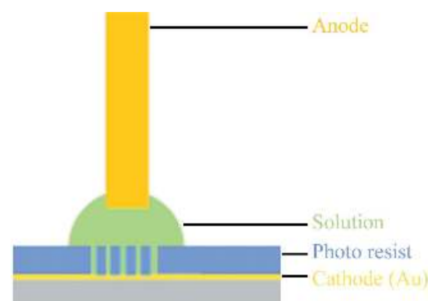

Figure 1
Schematic map of the electrodeposition instrument for Au zone construction of FZP.

We designed a pattern with all the essential characteristics whose fabrication requires a reduced amount of e-beam writer time: this enabled us to effectively evaluate the optimal dosage before the full FZP fabrication. We also verified that high e-beam voltage reduces electron scattering by the resist and the substrate. Indeed, patterns obtained with a lower voltage such as 30 keV clearly suffered from the scattering-induced proximity effect, reducing the accuracy and the aspect ratio.

Au was then electrodeposited in the resist pattern trenches. As mentioned, the special electrodeposition method (see Fig. 1) was similar to LECD. Specifically, the anode was a Pt rod of diameter 1 mm, protected by epoxy except for its end that was machined to expose a smooth and clean surface. The anode was aligned with the FZP resist pattern (the cathode) leaving a ~5 mm gap. A small volume, ~1 mm^3, of electrodeposition solution (ECF-77A-S, CHEMCAT Co.) was injected into the gap using a pipette to facilitate electrodeposition. Current pulses of duration 0.1 s, separated by 0.6 s, were found to produce best deposition results at room temperature. The current density was ~0.5 ASD (ampere per square decimeter). After completion of the electrodeposition, all the remaining resist was removed with acetone.

The success of electrodeposition on the nanometer scale critically depends on the selection of the electrolyte and of the applied current density. Conventional electrolytes are typically cyanide-based; they can attack the PMMA and degrade the pattern (Watanabe *et al.*, 1999). After extensive tests, we selected instead a sulfite-base electrolyte.

The pulsed current mode of electrodeposition was found to be better than the DC current mode for producing nanocrystalline structure (Chen & Wan, 1989) and more suitable for filling the narrow outer zone trenches. Since the diffusion length of Au in the electrolyte is larger than the outermost FZP zone width, the deposition is quickly terminated before the slow diffusion of Au ions is resupplied. The generation of hydrogen bubbles owing to the current supply to the electrode

without sufficient metal ions accentuates this problem leading to inhomogeneous deposition for different zones. The problem was solved by the pulsed current mode with an optimized time structure. In our case a current density of 0.2 ASD within a 0.1 s-long pulse separated by 0.6 s off periods produced optimal results.

The resolution and efficiency of FZPs fabricated using this procedure, with 30 nm outermost zone width and 450 nm thickness and a focal length of 2.7 cm, were tested at the transmission X-ray microscope (TXM) beamline (BL01B) of the National Synchrotron Radiation Research Center (NSRRC) in Hsinchu, Taiwan. A superconducting wavelength shifter source provided a photon flux of 4.5×10^{11} photons s^{-1} (0.1% bandwidth)$^{-1}$ in the photon energy range 5–20 keV and the X-ray beam was focused by a toroidal mirror with a 1:1 focal ratio before reaching the first TXM condenser. The photon energy for our test, 8 keV, was provided by a double-crystal monochromator. A test sample fabricated by the same process as the FZP was used to evaluate the image resolution.

3. Results and discussions

The availability of highly coherent X-rays from synchrotrons, free-electron lasers and laser plasma sources has stimulated a strong demand for suitable hard-X-ray FZPs. As already mentioned, the FZP resolution depends on the smallest zone width and therefore on the fabrication accuracy. The FZP focuses the beam by creating the required phase shift between adjacent transmitting zones. However, this mechanism requires sufficiently thick non-transmitting zones. A plot of the calculated efficiency *versus* zone thickness at 8 keV photon energy is shown in Fig. 2. A low aspect ratio structure with an Au thickness of 100 nm would give an efficiency of <0.4%, whereas with an Au thickness of 500 nm an efficiency of >8% can be obtained. In general terms, >450–500 nm Au lines are required for multi-keV X-rays. The simultaneous demands of small line width and large line thickness make X-ray FZP production one of the most challenging nanofabrication technologies. The need for a high aspect ratio is in fact the major factor that prevented hard-X-ray microscopy from obtaining high-resolution and high-quality images as that achieved by soft-X-ray microscopy.

The well defined FZP patterning requires a 'top-down' lithography approach and rules out the popular 'bottom-up' nanofabrication methods. By using e-beam lithography and electrodepositon we avoided the complicated use of lithography masks. The high accelerating voltage of the e-beam writer reduced the negative scattering effects leading to an accurately defined FZP pattern with a vertical side wall for the 30 nm outermost zone. In order to maintain this pattern accuracy, we optimized the resist developing process specifically minimizing swelling effects. In the final electrodeposition process, besides the aforementioned specially designed geometry, we used a non-cyanide-based electrolyte to reduce the simultaneous damage to the photoresist. We will now discuss in detail some of the crucial features of the fabrication strategy.

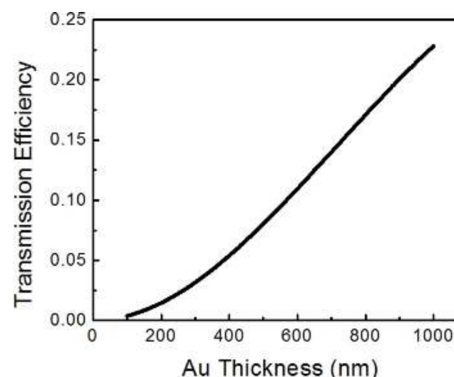

Figure 2
Calculated efficiency as a function of the Au thickness for a zone plate designed to work at 8 keV photon energy.

3.1. E-beam dosage optimization

This optimization is not easy owing to the wide range of line widths and densities in the FZP pattern. Our experience

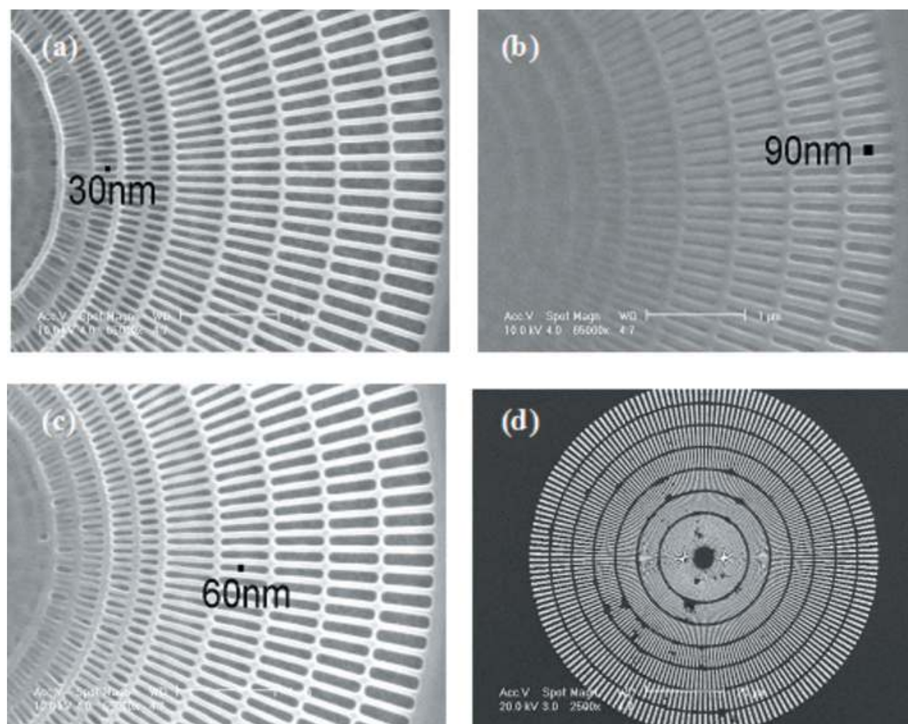

Figure 3
Scanning electron microscope (SEM) images of the test sample with optimized dose for patterning different lines: (*a*) 650 μC cm^{-2} for 30 nm line, (*b*) 380 μC cm^{-2} for 90 nm line, (*c*) 474 μC cm^{-2} for 60 nm line, (*d*) pattern with Au structure after electrodeposition.

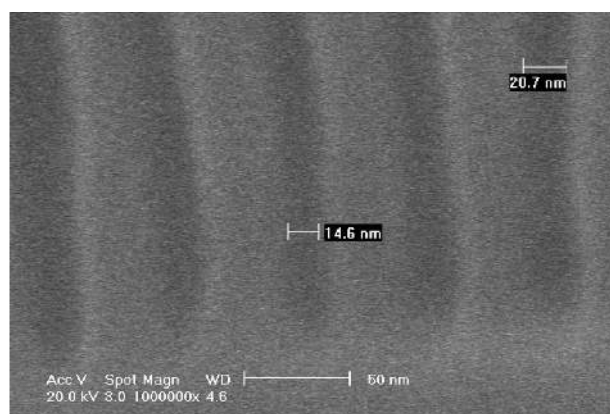

Figure 4
SEM image of PMMA A6 with 14.6 nm line width after EBL writing.

indeed shows that one dosage cannot be applied to all line widths without resulting in collapsed or swelled structures (Dobisz *et al.*, 2000). High-resolution e-beam writing of a FZP pattern with thousands of zones is a very time-consuming task: the consequent high cost makes trial-and-error optimization impractical. Optimization by patterning only a partial FZP structure with reduced e-beam writing time does not guarantee that the results are valid for the entire device.

The fabrication results are shown in Fig. 3. We confirmed that the optimal dose does vary with the line width below the 100 nm level. For example, the optimized dose for 30 nm lines is 37% higher than for 60 nm lines. The general tendency is higher doses within the 450–550 $\mu C\,cm^{-2}$ range for smaller line widths.

With our optimization we achieved (Fig. 4) a patterning accuracy of $\sim$14.6 nm with a 450 nm-thick PMMA A6 resist. To the best of our knowledge, no similar aspect ratio and high-density structure has previously been obtained below the 20 nm level. Therefore, the high e-beam voltage is indeed critical for our final objective of a 30 nm line width after electrodeposition.

3.2. Definition of the FZP pattern

3.2.1. Optimization of the resist bake-out. Commonly used baking parameters for PMMA resists, such as those empirically determined for thin structures (at 408 K for 2 h), are inadequate for high-aspect-ratio nanostructures. We attribute this poor result to the incomplete removal of the residual solvent in the resist that makes it too soft for the subsequent pattern development process. A higher temperature and longer bake-out time, such as 453 K for 24 h, was found to eliminate this problem.

Fig. 5 shows FZP pattern results obtained using different bake-out temperatures. With optimized bake-out parameters, the outer zones were closer to the desired rectangular shape, as shown in Fig. 5(*b*), rather than of elliptical shape as shown in Fig. 5(*a*). The width of the patterned lines was also more accurate.

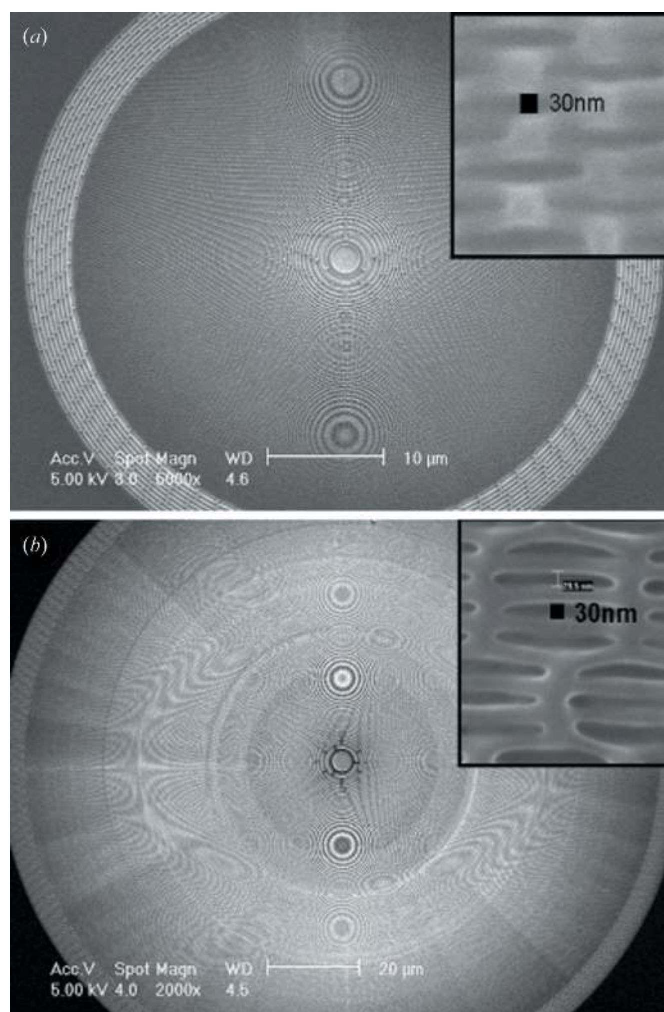

Figure 5
SEM images of a FZP pattern on PMMA A6 resist under different bake-out conditions after development: (*a*) 408 K for 2 h, (*b*) 453 K for 24 h.

3.2.2. Development of the patterned resist. The typical developer for PMMA after EBL patterning is a 1:3 mixture of MIBK and IPA. MIBK is a strong solvent with high sensitivity; however, it can negatively affect the resolution and accuracy of nanoscale patterns (Dobisz *et al.*, 2000). We therefore sought a developer with no MIBK and found that mixing IPA and water in a 7:3 ratio results in the best pattern accuracy after development. This developer produced the accurate FZP patterns with 30 nm outermost zone and 450 nm thickness shown in Fig. 6.

3.3. Electrodeposition

The EBL process yielded FZP patterns with high accuracy and vertical side wall. However, these trenches made it difficult to remove the remaining photoresist with the common lift-off procedure. Electrodeposition (rather than vapor deposition) provided the best overall solution.

Our specially designed electrodeposition bath (Fig. 1) provided several advantages. First, the area and the shape of the anode is similar to the FZP dimensions leading to an easier

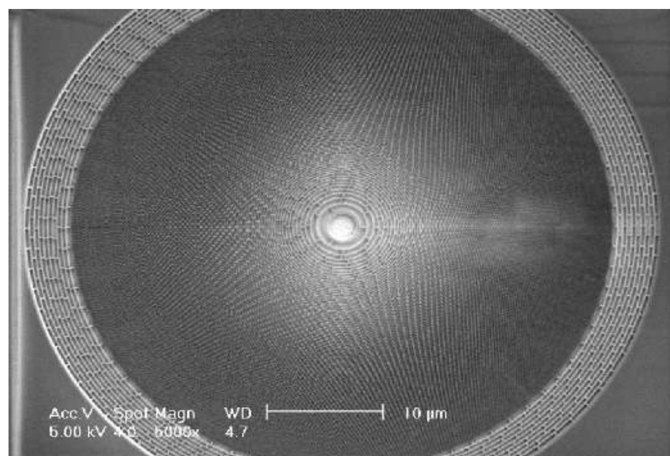

Figure 6
FZP pattern on PMMA A6 resist after using IPA and water mixture (7:3) as developer and a development time of 60 s.

control of the electric field distribution without the complications created by a large area outside the FZP or the sacrificial electrode (Jangidze *et al.*, 2007). Second, the small electrolyte volume, more than sufficient for the actual Au ion consumption, reduced the unwanted deposition on the area outside the FZP structures, and guarantees identical ion concentration and quality of the electrolyte by preventing it from being contaminated by the remaining part of the sample on the anode. The small volume is also likely to limit the uncontrollable convection.

Our electrodeposition geometry was successfully used to produce 1000 nm-thick Au FZP structures with an 80 nm-wide outermost zone, and >450 nm-thick structures with a 30 nm outermost zone (see Fig. 7). The corresponding aspect ratios of both FZPs were >12, demonstrating that our LECD-like (or 'dip-pen-like') electrodeposition approach is an excellent strategy for the fabrication of high-aspect-ratio devices.

3.4. Tests of the FZPs performances in TXM

A set of 450 nm-thick Au FZPs with 30 nm outermost zone width produced using the above fabrication procedures were tested for their performances in synchrotron X-ray microscopy using the full-field imaging set-up of the TXM station at the NSRRC BL01B beamline. The micrographs in Fig. 8 show results for a test sample (spoke shape test pattern as in Fig. 2 fabricated using our procedure) obtained at 2.7 cm from the TXM FZP objectives. Small ~40 nm-wide lines in the test samples can be identified in the images.

4. Conclusions

We have demonstrated that after careful optimization of many different parameters our fabrication method, combining sub-10 nm EBL and electrodeposition, can overcome the challenges of combining high accuracy/resolution and a high aspect ratio. Specific optimizations included the e-beam dosage, the temperature control of the resist bake-out, several issues concerning the resist developer and the electrolyte, and

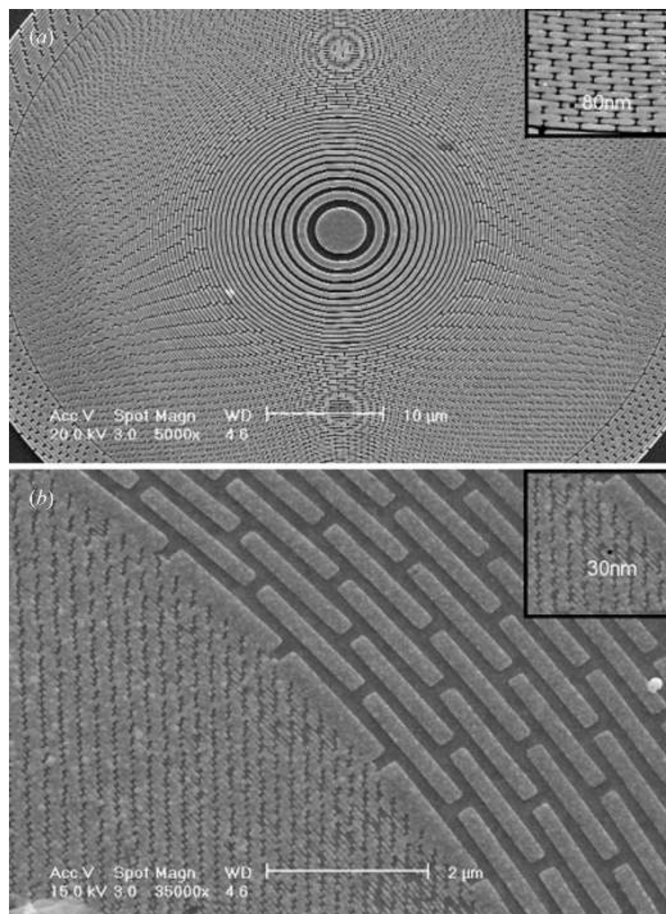

Figure 7
SEM images of FZP Au structures after electrodeposition. (*a*) 80 nm outermost zone width and 1000 nm thickness. (*b*) 30 nm outermost zone and 450 nm thickness.

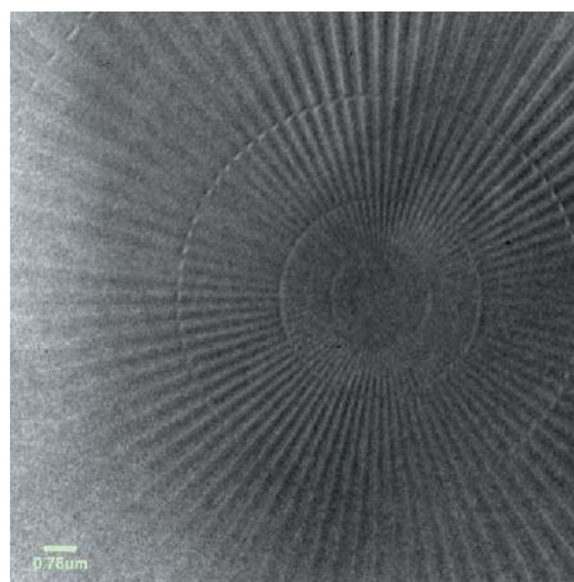

Figure 8
TXM images of test patterns obtained at a position 2.7 cm from the FZP objective.

a careful design of the electrodeposition geometry. The initial results of this approach include a 450 nm-thick FZP with 30 nm minimum zone width and a FZP able to magnify transmission X-rays images yielding 40 nm resolution. This approach can find more general applications in the nanofabrication of high-aspect-ratio devices.

This work is supported by the National Science and Technology Program for Nanoscience and Nanotechnology, the Thematic Research Project of Academia Sinica, the National Synchrotron Radiation Research Center (Taiwan), the Creative Research Initiatives (Functional X-ray Imaging) of MOST/KOSEF, the Swiss National Science Foundation and the Center for Biomedical Imaging (CIBM) in Lausanne (funded in part by the Leenaards and Jeantet Foundations). The Core Facility for Nanoscience and Nanotechnology at Academia Sinica and NSRRC are acknowledged for the use of the equipment.

References

Anderson, E. H., Olynick, D. L., Chao, W. L., Harteneck, B. & Veklerov, E. (2001). *J. Vac. Sci. Technol. B*, **19**, 2504–2507.

Attwood, D. (1999). *Soft X-rays and Extreme Ultraviolet Radiation: Principles and Applications*, pp. 337–394. Cambridge University Press.

Brambley, D. R. & Bennett, R. H. (1996). *GEC J. Res.* **13**, 42–53.

Chen, C. J. & Wan, C. C. (1989). *J. Electrochem. Soc.* **136**, 2850–2855.

Dobisz, E. A., Brandow, S. L., Bass, R. & Mitterender, J. (2000). *J. Vac. Sci. Technol. B*, **18**, 107–111.

Hambach, D., Peuker, M. & Schneider, G. (2001). *Nucl. Instrum. Methods Phys. Res. A*, **467**, 877–880.

Jangidze, L. B., Tavkhelidze, A. N., Tetradze, M. O. & Devidze, T. N. (2007). *Russ. Microelectron.* **36**, 116–119.

Lo, T. N., Chen, Y. T., Chiu, C. W., Liu, C. J., Wu, S. R., Lin, I. K., Su, C. I., Chang, W. D., Hwu, Y., Shew, B. Y., Chiang, C. C., Je, J. H. & Margaritondo, G. (2007). *J. Phys. D*, **40**, 3172–3176.

Manjkow, J., Papanu, J. S., Soong, D. S., Hess, D. W. & Bell, A. T. (1987). *J. Appl. Phys.* **62**, 682–688.

Olzierski, A. & Raptis, I. (2004). *Microelectron. Eng.* **73–74**, 244–251.

Said, R. A. (2003). *Nanotechnology*, **14**, 523–531.

Seol, S. K., Pyun, A. R., Hwu, Y., Margaritondo, G. & Je, J. H. (2005). *Adv. Funct. Mater.* **15**, 934–937.

Watanabe, H., Hayashi, S. & Honma, H. (1999). *J. Electrochem. Soc.* **146**, 574–579.

Yasin, S., Hasko, D. G. & Ahmed, H. (2002). *Microelectron. Eng.* **61–62**, 745–753.

Yin, G. C., Song, Y. F., Tang, M. T., Chen, F. R., Liang, K. S., Duewer, F. W., Feser, M., Yun, W. B. & Shieh, H. P. D. (2006). *Appl. Phys. Lett.* **89**, 221122.